BJ www.biochemj.org

BJ Plant

Biochem. J. (2012) **442**, 57–63 (Printed in Great Britain) doi:10.1042/BJ20111498

The pH sensor of the plant K^+-uptake channel KAT1 is built from a sensory cloud rather than from single key amino acids

Wendy GONZÁLEZ*†[1,2], Janin RIEDELSBERGER†[1], Samuel E. MORALES-NAVARRO*, Julio CABALLERO*, Jans H. ALZATE-MORALES*, Fernando D. GONZÁLEZ-NILO*‡ and Ingo DREYER†§[2]

*Centro de Bioinformática y Simulación Molecular, Universidad de Talca, 2 Norte # 685, 3465548, Talca, Chile, †Universität Potsdam, Institut für Biochemie und Biologie, Heisenberg-Group BPMPB, Karl-Liebknecht-Strasse 24/25, Haus 20, D-14476 Golm, Germany, ‡Centro Interdisciplinario de Neurociencia de Valparaíso, Valparaíso, Chile, and §Centro de Biotecnología y Genómica de Plantas, Universidad Politécnica de Madrid, Campus de Montegancedo, Carretera M-40, km 37.7, E-28223-Pozuelo de Alarcón (Madrid) Spain

The uptake of potassium ions (K^+) accompanied by an acidification of the apoplasm is a prerequisite for stomatal opening. The acidification (approximately 2–2.5 pH units) is perceived by voltage-gated inward potassium channels (K_{in}) that then can open their pores with lower energy cost. The sensory units for extracellular pH in stomatal K_{in} channels are proposed to be histidines exposed to the apoplasm. However, in the *Arabidopsis thaliana* stomatal K_{in} channel KAT1, mutations in the unique histidine exposed to the solvent (His^{267}) do not affect the pH dependency. We demonstrate in the present study that His^{267} of the KAT1 channel cannot sense pH changes since the neighbouring residue Phe^{266} shifts its pK_a to undetectable values through a cation–π interaction. Instead, we show that Glu^{240} placed in the extracellular loop between transmembrane segments S5 and S6 is involved in the extracellular acid activation mechanism. Based on structural models we propose that this region may serve as a molecular link between the pH- and the voltage-sensor. Like Glu^{240}, several other titratable residues could contribute to the pH-sensor of KAT1, interact with each other and even connect such residues far away from the voltage-sensor with the gating machinery of the channel.

Key words: *Arabidopsis thaliana*, channel protein structure, channel protein–proton interaction, KAT1, pH regulation, potassium chanel.

INTRODUCTION

Stomata are pore structures found in the epidermis of plants. They optimize the uptake of CO_2 and loss of water vapour. Stomatal opening and closure is regulated by the turgor pressure of two guard cells that surround the stomatal pore [1]. Potassium (K^+) flux across the membrane is fundamental for the turgor-driven volume changes in guard cells. Specifically, K^+ uptake through inwardly rectifying channels (K_{in} channels) is essential for stomatal opening; a process accompanied by the acidification of the apoplast [2,3]. K^+ uptake depends on H^+-ATPase activity generating a sufficiently hyperpolarized membrane voltage, which provides an inward-directed electrochemical driving force for K^+ and opens the K_{in} channel gate [4]. K_{in} channels, besides opening upon hyperpolarization, sense through a protein-intrinsic pH-sensor the extracellular proton increase generated by H^+-ATPases [2,5,6]. Extracellular protons shift the voltage-dependence of guard cell K_{in} channels to more positive voltages and thereby facilitate K^+ uptake [7].

K_{in} channels display high sequence homology with animal *Shaker* channels. Each subunit possesses a six-segment (S1–S6) membrane-spanning topology. A selectivity filter segment (comprising the triad of GYG residues) [8], linking the S5 and S6 segments, forms the outer portion of a pore and confers the potassium-selectivity characteristics on the channel. Functional channels comprise four of these subunits, each one containing an intrinsic voltage sensor, which is composed primarily of charged amino acid residues of the S2, S3 and S4 segments [9].

Mutational analysis by Hoth et al. [6] allowed relating acid activation in KST1, a K_{in} channel from *Solanum tuberosum* (potato) guard cells, to two extracellular histidines. One histidine is located within the linker between the transmembrane helices S3 and S4 (His^{160}), and the other histidine is three amino acids outside the selectivity filter triad (His^{271}). The histidine from the GYGDXH motif is conserved among K_{in} channels. The conservation of this amino acid suggests that it represents a common entity of an extracellular pH-sensor [6] of plant K^+-uptake channels. To test this hypothesis, the guard cell K_{in} channel KAT1 from *Arabidopsis thaliana* was studied with respect to the structural basis for its acid activation. Surprisingly, the pH-dependent gating of KAT1 was not affected by mutation of this highly conserved histidine residue, suggesting that the two guard cell K_{in} channels KAT1 and KST1 have distinct molecular bases for acid activation [7].

In the present study, we came back to the structural aspects of extracellular acid activation of KAT1. Using site-directed mutagenesis, electrophysiology, yeast complementation, molecular simulation and quantum mechanics, we have shown that a glutamic acid residue (Glu^{240}) is involved in the extracellular acid activation mechanism. Furthermore, we have shown that the histidine of the GYGDXH motif cannot work as pH-sensor in KAT1 because it is interacting with the neighbouring phenylalanine (X position in the motif). From our combined results we conclude that the pH-sensor of KAT1 is built from a sensory cloud connecting different functional parts of the protein rather than single key amino acids.

EXPERIMENTAL

Molecular genetics and expression

KAT1 mutation, expression and analysis used standard molecular genetic methods. Site-directed mutations were generated as

Abbreviations used: CHARMM, Chemistry at HARvard Macromolecular Mechanics; HERG, human *ether-a-go-go*-related gene; K_{in} channel, inwardly rectifying potassium channel; SCF, self-consistent reaction field.

[1] These authors contributed equally to this work.

[2] Correspondence may be addressed to either of these authors (email wgonzalez@utalca.cl or ingo.dreyer@upm.es).

described previously [10]. All mutants were verified by sequencing. For expression, the coding regions of wild-type and mutant channels were cloned into the vector pGEMHE and cRNA was synthesized using T7 polymerase (mMessage mMachine, Ambion Europe). For expression in oocytes, stage V and VI oocytes were taken from *Xenopus laevis* and maintained at 18 °C in modified Barth's medium containing 96 mM NaCl, 2 mM KCl, 1 mM $CaCl_2$, 1 mM $MgCl_2$ and 10 mM Hepes/NaOH (pH 7.4). Oocytes were defolliculated by collagenase treatment (2 mg/ml, type IA, Sigma). Defolliculated oocytes were injected with 40 ng (1 μg/μl) of cRNA using a solid displacement injector (Picospritzer III, Parker Instrumentation) and kept at 18–20 °C. Control oocytes were injected with 40 nl of deionized water.

Electrophysiology

Whole-cell currents were measured under voltage clamp (Turbo TEC-10CX; NPI Electronic) with a two-electrode clamp circuit and virtual ground. Voltage control, data acquisition and data analyses were carried out using the Pulse/PulseFit software (HEKA, Lambrecht/Pfalz). Measurements were performed in bath solutions containing 1 mM $CaCl_2$, 2 mM $MgCl_2$, 30 mM KCl and 70 mM NaCl buffered with 10 mM Tris/Mes (pH 5–6) and 10 mM Tris/Mes (pH 7–9) to obtain solutions with six different pH values (pH 5, 5.6, 6, 7, 8 and 9). Measurements were repeated routinely at the end of each treatment with the addition of 10 mM CsCl to distinguish K^+ currents and any background, non-selective leak. In experiments where very negative voltages (< -170 mV) were tested, 1 mM $LaCl_3$ was added to the bath solution to efficiently suppress possible endogenous currents at these voltages [11].

Data analysis

To standardize comparisons of wild-type with mutant channel currents, their relative conductance was obtained in two-step pulse experiments. In a first pulse (variable voltage V), channels were activated followed by a tail-pulse (non-variable voltage V_T). The current measured at the end of the first pulse is the steady-state current I_{SS}. The current measured at the onset of the tail-pulse, tail current I_T, can be expressed as

$$I_T(\mathrm{V}) = N \times \mathrm{i}(V_T) \times P_{open}(\mathrm{V}) \quad (1)$$

where $P_{open}(\mathrm{V})$ is the open probability of the channel at the end of the first pulse. Thus the tail current is proportional to the open probability $P_{open}(\mathrm{V})$. The resulting curves were fitted such that:

$$I_T(\mathrm{V}) = I_{max}/\{1 + \exp[-(V - V_{1/2})/V_S]\} + \mathrm{offset} \quad (2)$$

where I_{max} is the maximum current, V is the voltage of the activation pulse, $V_{1/2}$ is the voltage giving half-maximal conductance, V_S is the voltage-sensitivity coefficient, and the offset parameter is a constant. Fittings were carried out using a Marquardt–Levenberg algorithm [12]. Current records were corrected for background current, estimated as a linear leak component from measurements between -130 and -160 mV after substituting Cs^+ for K^+ to block the K^+ channels. Measurements were discarded when the maximum leak current exceeded 5 % of the maximum current in the steady state.

Yeast complementation

For complementation growth tests, the yeast strain Wagf2 (Δ*trk1,2*-mutant) with a deficiency in low- and high-affinity K^+ uptake was used [13]. The KAT1 wild-type gene and the two mutated genes KAT1-F266L and KAT1-E240Q-F266L-H267R were cloned into pFL61 containing the *URA3* gene as a selection marker [14]. Selection minimal medium was prepared as described in [15]. The pH was adjusted to pH 5 using 10 mM Mes/Tris and to pH 8 using 10 mM Mes/Tris. Yeast transformations were carried out using the Frozen-EZ Yeast Transformation II™ Kit (Zymo Research/Hiss Diagnostics) and transformed yeast cells were selected on minimal medium containing 50 mM K^+. Complementation growth tests were performed as described in [15] with solid and liquid minimal media containing 0.5 mM K^+ and an adjusted to pH 5 or 8 respectively. Yeast growth in liquid medium was described by the equation:

$$D_{600}(t) = (D_\infty \times D_0)/[D_0 + (D_\infty - D_0) \times \exp(-t/\tau)] \quad (3)$$

where D_0 and D_∞ denote the attenuances at $t = 0$ and infinity respectively [15].

Molecular simulation

Basic structural models of plant K^+ channels were generated previously [16,17]. To study the structural basis of extracellular acid activation of KAT1, we added to its molecular model the extracellular loop between the transmembrane segments S5 and S6 (residues 223–238) that were not included before in the model. The model was embedded in a POPC (1-palmitoyl-2-oleoyl-*sn*-glycero-3-phosphocholine) membrane, minimized and equilibrated as described in [16]. Minimization and equilibration were performed using the NAMD program [18], using CHARMM (Chemistry at HARvard Macromolecular Mechanics) force field [19]. As cation–π interactions are not included in CHARMM force field, we applied to the lateral chains of Phe^{266} and His^{267} a harmonic restraint of 5 kcal/mol (1 kcal = 4.184 kJ) during equilibration.

A model of the mutant F266L-H267R was generated *in silico* in the open state. F266L-H267R was built using the 'mutate' plug-in of the VMD program [20] on the basis of the enlarged homology model of KAT1. The KAT1-F266L-H267R mutant channel was inserted into the membrane, minimized and equilibrated following the same protocol as applied for wild-type KAT1.

pK_a quantum mechanics calculations

Theoretical pK_a values are usually obtained considering thermodynamic cycles, which also can involve some experimental values. We considered some of the most common thermodynamic cycles reported previously [21,22]. All of them combine gas-phase and liquid-phase calculations in order to calculate aqueous deprotonation free energy as:

$$\Delta G_{aq} = \Delta G_{gas} + \Delta\Delta G_{solv} \quad (4)$$

where ΔG_{gas} and $\Delta\Delta G_{solv}$ are the gas-phase free energy and the aqueous solvation free energy differences between conjugate base and acid respectively.

In the thermodynamic cycle used in the present study, ΔG_{gas} and $\Delta\Delta G_{solv}$ are expressed as:

$$\Delta G_{gas} = G_{gas}(\mathrm{H}^+) + G_{gas}(A^{q-1}) - G_{gas}(\mathrm{AH}^q) \quad (5)$$

and

$$\Delta\Delta G_{solv} = \Delta G_{solv}(H^+) + \Delta G_{solv}(A^{q-1}) - \Delta G_{solv}(AH^q) \quad (6)$$

The values for $G_{gas}(H^+)$ of -6.28 kcal/mol and $\Delta G_{solv}(H^+)$ of -267.9 kcal/mol were derived experimentally previously [23,24]. As the calculation of ΔG_{gas} and ΔG_{solv} uses different reference pressure states [1 atm (=101.325 kPa) and 1 M respectively], the ΔG_{gas} reference state (24.46 L at 298.15 K) needs to be converted using the equation:

$$\Delta G_{gas}(1\ M) = \Delta G_{gas}(1\ atm) + RT\ln(24.46) \quad (7)$$

Eventually, the pK_a was obtained from eqn (8):

$$pK_a = \Delta G_{aq}/2.303\,RT \quad (8)$$

All calculations were performed with the quantum mechanics module Jaguar included in Schrödinger software. The Becke3LYP density functional hybrid method [26] in combination with 6–31G**++ basis set were used for all gas-phase calculations. For liquid-phase calculation the 6–31G* was used. Solvation-free energies were obtained with a SCF (self-consistent reaction field) method given by a standard Poisson–Boltzmann solver [27,28] implemented in the Jaguar module software. Jaguar first calculates the usual gas-phase wave function, and from that the electrostatic potential, and finally fits that potential to a set of atomic charges. These charges are passed to the Poisson–Boltzmann solver, which then determines the reaction field by numerical solution of the Poisson–Boltzmann equations. The solvent is finally represented as a layer of charges at the molecular surface (which serves as a dielectric continuum boundary). These solvent point charges are returned to Jaguar's SCF program, which performs another quantum mechanical wave function calculation, incorporating the solvent charges. This process is repeated until self-consistency is obtained. As solvent in aqueous solvation free energy calculations served water with a bulk dielectric constant of 80.37 and probe radius of 1.40 Å (1 Å = 0.1 nm).

RESULTS

KAT1-Glu^{240} plays an important role in extracellular pH-sensing

Activation of KAT1 is regulated by extracellular protons within an interval of approximately 4 pH units between pH 4 and pH 8 [7]. This range suggests that acidic residues such as aspartate and glutamate with a pK_a of approximately 4.1 could also account for acid activation in KAT1. We therefore screened our structural model of KAT1 [16,17] for extracellular acidic residues that could be involved in the pH-sensing mechanism and identified five glutamates and aspartates (Figure 1).

Mutations in four extracellular acidic residues KAT1-D221N, KAT1-E161R, KAT1-D277N and KAT1-D89N did not affect the pH-sensitivity (results not shown). In contrast, the mutant KAT1-E240Q exhibited a decreased pH-sensitivity compared with the wild-type. Whereas wild-type currents decreased by approximately 37 % at -160 mV upon a shift from pH 5 to pH 8 in the extracellular medium (Figure 2A), currents mediated by KAT1-E240Q did only by approximately 18 % (Figure 2B). This difference was also mirrored in a reduced difference in the half-maximal activation voltages $V_{1/2}$ (Figures 2C and 2D). Glu^{240} is placed in an extracellular loop between transmembrane segments S5 and S6 (Figure 1). Because this region is in close contact to the voltage-sensing module (S1–S4 [4]) it could represent a molecular link between the pH- and the voltage-sensor.

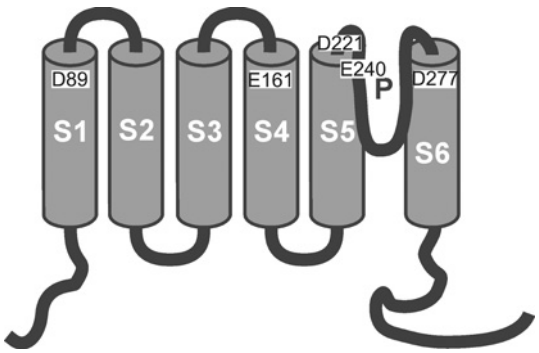

Figure 1 Putative extracellular acidic residues potentially involved in the acid activation mechanism of KAT1

S1 to S6 represent the transmembrane segments, and P is the pore helix between segments S5 and S6.

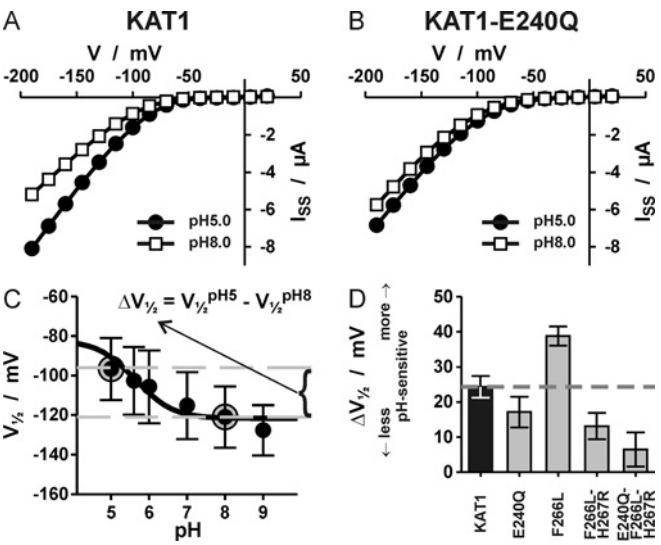

Figure 2 KAT1 mutants with altered pH-sensitivity

(**A**) Representative *I–V* relationship of KAT1 measured at pH 5.0 (circles) and pH 8.0 (squares). (**B**) Representative *I–V* relationship of the mutant KAT1-E240Q measured at pH 5.0 (circles) and pH 8.0 (squares). Currents were elicited from a holding voltage of $V_H = -20$ mV by 1 s voltage steps. Steady currents were measured at the end of the voltage pulse. (**C**) pH-dependence of the half-maximal activation voltage $V_{1/2}$ of KAT1. Results are means ± S.D. ($n = 3$). The continuous black line represents the best fit with the equation $V_{1/2} = V_\infty - V_S \cdot \ln[(10^{pH} + K_C)/(10^{pH} + K_0)]$ (6). The $\Delta V_{1/2}$ values displayed in (**D**) were calculated as difference between the $V_{1/2}$ values measured at pH 5 and at pH 8 (indicated by grey circles). (**D**) $\Delta V_{1/2}$ values of KAT1 and four mutants. Results are means ± S.D. ($n = 3$–5). Values above the broken grey line (KAT1 wild-type reference) indicate an increased pH-sensitivity and values below the broken grey line indicate a decreased sensitivity.

Mutation F266L potentiates pH-sensing of KAT1

A sequence alignment between guard cell K_{in} channels showed that the histidine in the GYGDXH motif is highly conserved. This pore histidine was identified as a major component of the acid activation mechanism of the channel KST1 [6], whereas in KAT1 it was apparently not involved [7]. Closer inspection now revealed that in the motif at position X a leucine is usually present. KAT1 is the only exception. There a phenylalanine (Phe^{266}) is found instead. We hypothesized that pH-dependent gating of KAT1 is not affected by mutations of the pore histidine [7] because an interaction between Phe^{266} and His^{267} shifts the pK_a of His^{267} outside the pH range ($5 < pH < 9$) tested. Indeed, the mutation F266L [29] increased the pH effect of KAT1 (Figure 2D)

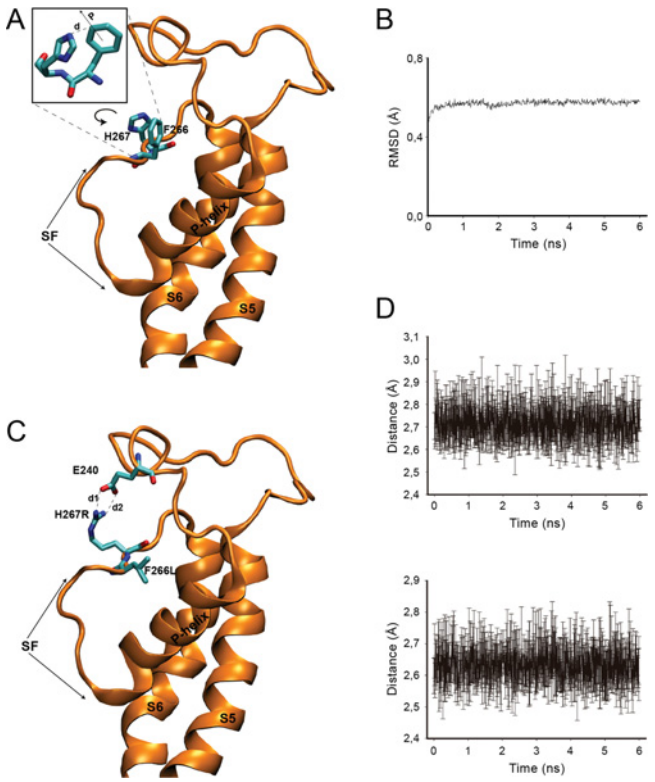

Figure 3 Position of key residues in the molecular models

(**A**) Position of KAT1-F266 and KAT1-H267 in the molecular model of wild-type KAT1. Representation of the pore from one KAT1 monomer; Phe^{266} and His^{267} are outside the selectivity filter (SF). Segments S5, S6 and the P-helix are explicitly displayed. Inset: expanded view of interacting Phe^{266} and His^{267}. $d = 4.5$ Å is the minimal distance from one of the atoms of the aromatic ring to the atom $N_{\varepsilon 2}$ in the histidine. $P = 2.75$ Å is equal to twice the radius of the aromatic ring. (**B**–**D**) Positions of Glu^{240}, and mutated residues F266L and H267R in the KAT1-F266L-H267R molecular model. (**B**) During a 6 ns equilibrated molecular dynamic simulation of KAT1-F266L-H267R the Glu^{240}, and mutated residues F266L and H267R adopted the positions shown in (**C**). Root mean square deviation (RMSD) was calculated with the VMD trajectory tool [20] using α-C atoms confirms equilibration over the 6 ns period. (**C**) Representation of the pore of one channel monomer. The mutated residues F266L and H267R are outside the selectivity filter (SF) and Glu^{240} is in the S5–S6 loop. S5, P-helix and S6 segment are explicitly displayed. (**D**) Time course of distance between Glu^{240} and H267R. During 6 ns of molecular simulation, the distances $d1$ (top) and $d2$ (bottom) between the oxygen atoms of the glutamate and the nitrogen atoms of the arginine are smaller than 3.2 Å.

suggesting that in the absence of the interaction with Phe^{266}, His^{267} may contribute to pH-sensing at physiological values.

The interaction between Phe^{266} and His^{267} could have a cation–π nature where the dominating component is the attraction of the positive charge (from a positive residue: arginine, lysine or histidine) towards the quadrupole created by the π–electron cloud of the aromatic ring [30]. In proteins, this type of interaction is frequently observed [31,32]. They are usually identified according to a distance and an angle criterion [33]. The distance criterion (d) requires that at least one of the atoms of the aromatic ring is located not further than 4.5 Å from the atom $N_{\varepsilon 2}$ carrying the positive charge of the histidine. The angle criterion demands the latter atom to be situated above the plane defined by the aromatic ring; more precisely, inside a cylinder of height of 4.5 Å, whose base includes the ring and has a radius (P) equal to twice the radius of the ring. In the molecular model of KAT1, Phe^{266} and His^{267} fulfil these two conditions (Figure 3A).

In order to estimate the shift in the pK_a value of His^{267} due to the strong cation–π interaction with Phe^{266}, we built some small molecular models of the histidine and its complex with the neighbouring phenylalanine. The histidine and phenylalanine residue models were represented by an imidazole and a benzene ring respectively. The initial atomic co-ordinates were taken from our structural model of KAT1. First, the theoretical pK_a value for the histidine alone was estimated by quantum mechanics calculations at DFT (density functional theory) level. Then, the pK_a value of the histidine was re-estimated, but this time in the presence of the benzene ring of the phenylalanine, with which it establishes the cation–π interaction. As shown in Table 1, the theoretical pK_a value predicted for the isolated histidine is in good agreement (deviation of 0.76 pK_a unit) with the experimental value reported for the imidazole ring [34]. In the presence of Phe^{266}, however, the strong cation–π interaction between the positive charge of $N_{\varepsilon 2}$ in His^{267} and the rich electronic cloud of the benzene ring of Phe^{266} increases the free energy needed to subtract the acidic proton of the histidine. The theoretical pK_a value determined for the model complex between the imidazole and benzene rings is approximately 10.27, indicating a difference between the pK_a values of free histidine and the histidine–phenylanaline complex of approximately 3.32 pK_a units (Table 1). Thus, under the (physiological) pH values tested, the histidine would remain protonated.

Table 1 Calculated pK_a values for model systems of His^{267} and the His^{267}–Phe^{266} complex

Model system	Experimental pK_a	Calculated pK_a	Error
His^{267} (imidazole ring)	6.95 [33]	7.71	0.76
His^{267}–Phe^{266} complex (imidazole–benzene rings)	–	10.27	–

Double mutant KAT1-F266L-H267R exhibits decreased pH-sensitivity

In line with our explanation of a cation–π interaction between His^{267} and Phe^{266}, the simple mutant KAT1-H267R showed the same pH-dependence as the wild-type [7]; in both cases histidine or arginine residues are trapped in a cation–π interaction. However, when we introduced the H267R mutation in the background of the previously described hypersensitive KAT1-F266L channel, the pH-sensitivity of the resultant double mutant diminished not only in comparison with KAT1-F266L but also in comparison with the KAT1 wild-type (Figure 2D). Thus disruption of the cation–π interaction by the mutation F266L releases the histidine to contribute to the sensing of physiological pH changes.

In the double mutant KAT1-F266L-H267R, however, the arginine released interferes with other components of the pH-sensor. Molecular dynamics simulation of the KAT1-F266L-H267R homology model proposes an interaction between the arginine residue and Glu^{240}. Using the VMD 'salt bridge' plug-in (http://www.ks.uiuc.edu/Research/vmd/plugins/saltbr/) we could identify during 6 ns of molecular dynamics simulation of KAT1-F266L-H267R a salt bridge between the arginine and Glu^{240}. A salt bridge is considered to be formed if the distance ($d1$, $d2$) between the oxygen atoms of an acidic residue (glutamate) and the nitrogen atoms of a basic residue (arginine) are within a distance of 3.2 Å (Figures 3B–3D).

Triple mutant KAT1-E240Q-F266L-H267R is almost pH-insensitive

In a next step, we intended to disrupt the salt bridge by neutralizing the charge at Glu^{240} by replacing it with glutamine.

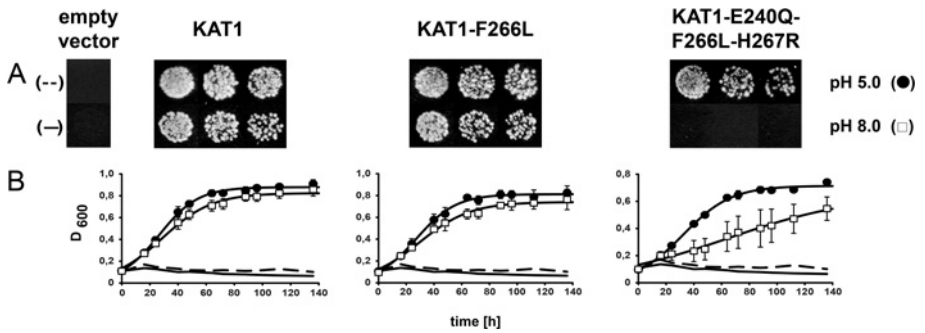

Figure 4 Growth tests using the potassium-uptake-deficient yeast strain Wagf2

The empty vector, the wild-type channel KAT1 and the two mutated channels KAT1-F266L and KAT1-E240Q-F266L-H267R were transformed into Wagf2 and the resulting growth behaviour on solid (**A**) and in liquid (**B**) media at different pH values was analysed. (**A**) Drop tests on solid medium. Transformed yeast cells were incubated overnight in liquid cultures containing 50 mM K^+. The cells were harvested and washed three times and the D_{600} (attenuance) of the cell suspension was set to 0.1 (left spot), 0.05 (middle spot) and 0.01 (right spot). Then 10 μl of these cell suspensions were dropped out on solid medium with pH 5 or pH 8 containing 0.5 mM K^+. Plates were incubated for 5 days at 30°C. (**B**) Growth test in liquid medium. Transformed yeast cells were treated as described in (**A**). Liquid medium with pH 5 or pH 8 containing 0.5 mM K^+ was inoculated with the yeast cell suspension so that all liquid cultures have an initial D_{600} of approximately 0.1. The cultures were incubated in a shaker at 30°C and 190 rev./min. The D_{600} was measured at the indicated time points. Lines representing the best fit with eqn (6). Shown results are means ± S.D. for at least three independent samples.

And, indeed, the triple mutant KAT1-E240Q-F266L-H267R was almost insensitive to pH changes in the tested interval (Figure 2D).

Yeast complementation

Finally, we tested the physiological implications of the modified pH-sensing properties by comparing the KAT1 wild-type with a hyper- (KAT1-F266L) and a hypo- (KAT1-E240Q-F266L-H267R) sensitive mutant in their performance to complement the potassium-uptake-deficient yeast strain Wagf2 (Δ*trk1*,*2*-mutant). Yeast growth was analysed under low K^+ conditions in drop test experiments on solid medium (Figure 4A) and growth kinetics were monitored in liquid culture (Figure 4B). At pH 5, all three channels facilitated yeast growth in a similar manner, albeit liquid yeast cultures expressing KAT1 mutants saturated at slightly lower (KAT1-F266L) or significantly lower (KAT1-E240Q-F266L-H267R) cell densities. When, however, the medium was strongly buffered to pH 8 the hyposensitive mutant KAT1-E240Q-F266L-H267R was far less efficient than the wild-type or the hypersensitive mutant KAT1-F266L. These results demonstrate *in vivo* the relevance of the pH-sensing mechanism of a K^+ channel in a living cell. We may speculate that proper adjustment of the voltage-dependence of the channel ($V_{1/2}$) balances the need for an open channel for K^+ uptake with the drawback of opening a potential K^+-efflux pathway under unfavourable energetic conditions. The pH-sensor thus links the activity of the K^+ channel to the activity of the H^+-ATPase, which in turn provides the energy for K^+ uptake. Maladjustment would result in the case of hypersensitive mutants in a too rigid limitation of K^+ uptake and in the case of hyposensitive mutants in a too casual control of potential K^+ efflux. In yeast, K^+ uptake is integrated over time. Therefore a reduced K^+-uptake potential (KAT1-F266L) might be more easily compensated than an increased potential of K^+ efflux (KAT1-E240Q-F266L-H267R).

DISCUSSION

All ion channels studied to date are regulated to a certain degree by protons [35]. In most cases acidification reduced ion current, either by blocking of the pore or alteration of channel gating [36–38]. In contrast, steady-state currents of guard cell K_{in} channels increase upon acidification of the apoplasm [2], caused by a shift of the $V_{1/2}$ to more positive voltages with decreasing extracellular pH [6,7]. In KAT1, the shift of $V_{1/2}$ upon an acidification from pH 8 to pH 5 is approximately 25 mV. This pH-dependent shift depends on the extracellular Glu^{240} (Figure 2). Previous studies have shown that KAT1 operates at more acidic pH values than its homologous channel in potato, KST1, pointing to the contribution of acidic amino acids such as aspartate or glutamate to the pH-sensor of KAT1 [7]. Residue KAT1-Glu^{240} (KST1 harbours a glutamine at the same position) is located in the extracellular loop that connects the transmembrane segments S5 and S6. This loop could reach and interact with the voltage-sensing domain, as in the HERG (human *ether-a-go-go*-related gene) channel, where this region serves as a bridge of communication between the outer mouth and the voltage-sensor [39]. KAT1, as the other members of plant *Shaker* channels, shares a particular sequence and structure similarity with channels of the EAG subfamily [40], to which also HERG belongs. Both exhibit a S5–S6 extracellular loop longer than that of other K_v channels. And similarly to KAT1, mutations in the S5–S6 extracellular loop of HERG influence the $V_{1/2}$ of channel activation.

To mimic a protonated glutamate in the S5–S6 linker, we replaced Glu^{240} with glutamine. Protonation-mimicking versions of key residues keep the bacterial potassium channel KcsA, which is gated by intracellular acidic pH, in the open state [41]. The mutant KAT1-E240Q is less pH-sensitive than the wild-type KAT1 but it is still influenced by protons indicating that protonation of Glu^{240} is not essential for the extracellular pH-sensing mechanism of KAT1. However, the titratable side chain in Glu^{240} may contribute to a certain extent to the phenomenon.

For KST1, acid activation was related to a histidine residue in the consensus sequence GYGDXH [6,7,42]. In KAT1, the corresponding residue (His^{267}) was apparently not involved in the extracellular pH-sensing mechanism [7]. In the present study, by combining mutational analyses with molecular dynamics and quantum mechanics calculations, we provide an explanation for this difference between the two guard cell K_{in} channels: an interaction between His^{267} and its neighbouring Phe^{266} shifts the pK_a of the histidine to very high values in KAT1. KST1 has, like many other K_{in} channels, a leucine instead of the phenylalanine next to the histidine. When, in KAT1, Phe^{266} was replaced with leucine, the pH-sensitivity increased, suggesting that, in the case of KAT1-F266L, the histidine contributes to the pH-sensor. This hypothesis was further corroborated by

mimicking a constitutively protonated residue at the histidine position by the additional H267R mutation. The double mutant KAT1-F266L-H267R was far less pH-sensitive than KAT1-F266L. In contrast, in the presence of the phenylalanine, the histidine–arginine exchange did not influence the channel's pH-sensitivity (KAT1 compared with KAT1-H267R [7]). From these combined results we have to conclude that protonation of certain key residues is not relevant for the extracellular pH-sensing mechanism of KAT1; in contrast, several titratable amino acids contribute to the modification of channel activation. This hypothesis was further supported by the triple mutant KAT1-E240Q-F266L-H267R. We mimic the protonated glutamate form (E240Q) and a constitutively protonated histidine (H267R). This mutant is almost insensitive to pH changes but still exhibits a shift in $V_{1/2}$ upon an acidification from pH 8 to pH 5 by approximately 5 mV (Figure 2D).

In conclusion the present study indicates that, instead of single key amino acids, several titratable residues contribute to the pH-sensor of the plant K_{in} channel KAT1; many of them have not yet been identified. Nevertheless, we glimpse that these residues in the outer pore and in other extracellular linkers interact with each other and even connect such residues far away from the voltage-sensor with the gating machinery of the channel. Such a 'pH-sensory cloud' would equip plants with a high flexibility to adapt their K^+-uptake channels easily to many different environmental needs.

AUTHOR CONTRIBUTION

Wendy González and Ingo Dreyer designed research. Wendy González, Janin Riedelsberger, Samuel E. Morales-Navarro, Julio Caballero, Jans H. Alzate-Morales performed research. Wendy González, Janin Riedelsberger, Samuel E. Morales-Navarro, Julio Caballero, Jans H. Alzate-Morales, Fernando D. González-Nilo and Ingo Dreyer analysed data. Wendy González and Ingo Dreyer wrote the paper.

ACKNOWLEDGEMENTS

We thank Johanna Burgos and Antje Schneider for technical assistance.

FUNDING

This work was supported by the DAAD-CONICYT (Servicio Alemán de Intercambio Académico-Comisión Nacional de Investigación Científica y Tecnológica) AleChile project NiaPoc, the Fondo Nacional de Desarrollo Científico y Tecnológico (Chile) [grant number 11100373 (to W.G.)], the Abate Molina Excellence Award (to I.D.), the Deutsche Forschungsgemeinschaft [grant number DR 430/8] and a Heisenberg fellowship (to I.D.). J.R. is a recipient of doctoral fellowship from the Max-Planck Research School 'Primary Metabolism and Plant Growth'. S.E.M.N. is a recipient of a doctoral fellowship from CONICYT (Comisión Nacional de Investigación Científica y Tecnológica). The Centro Interdisciplinario de Neurociencia de Valparaíso is a Millennium Science Institute.

REFERENCES

1 Roelfsema, M. R. and Hedrich, R. (2005) In the light of stomatal opening: new insights into 'the Watergate'. New Phytol. **167**, 665–691
2 Blatt, M. R. (1992) K^+ channels of stomatal guard cells. Characteristics of the inward rectifier and its control by pH. J. Gen. Physiol. **99**, 615–644
3 Shimazaki, K., Iino, M. and Zeiger, E. (1986) Blue light-dependent proton extrusion by guard-cell protoplasts of *Vicia faba*. Nature **319**, 324–326
4 Dreyer, I. and Blatt, M. R. (2009) What makes a gate? The ins and outs of K_v-like K^+ channels in plants. Trends Plant Sci. **14**, 383–390
5 Véry, A. A., Gaymard, F., Boeseux, C., Sentenac, H. and Thibaud, J. B. (1995) Expression of a cloned plant K^+ channel in *Xenopus* oocytes: analysis of macroscopic currents. Plant J. **7**, 321–332
6 Hoth, S., Dreyer, I., Dietrich, P., Becker, D., Müller-Röber, B. and Hedrich, R. (1997) Molecular basis of plant-specific acid activation of K^+ uptake channels. Proc. Natl. Acad. Sci. U.S.A. **94**, 4806–4810
7 Hoth, S. and Hedrich, R. (1999) Distinct molecular bases for pH sensitivity of the guard cell K^+ channels KST1 and KAT1. J. Biol. Chem. **274**, 11599–11603
8 Doyle, D. A., Morais-Cabral, J., Pfuetzner, R. A., Kuo, A., Gulbis, J. M., Cohen, S. L., Chait, B. T. and MacKinnon, R (1998) The structure of the potassium channel: molecular basis of K^+ conduction and selectivity. Science **280**, 69–77
9 Gambale, F. and Uozumi, N. (2006) Properties of *shaker*-type potassium channels in higher plants. J. Membr. Biol. **210**, 1–19
10 Poree, F., Wulfetange, K., Naso, A., Carpaneto, A., Roller, A., Natura, G., Bertl, A., Sentenac, H., Thibaud, J. B. and Dreyer, I. (2005) Plant K_{in} and K_{out} channels: approaching the trait of opposite rectification by analyzing more than 250 KAT1-SKOR chimeras. Biochem. Biophys. Res. Commun. **332**, 465–473
11 Naso, A., Montisci, R., Gambale, F. and Picco, C. (2006) Stoichiometry studies reveal functional properties of KDC1 in plant *shaker* potassium channels. Biophys. J. **91**, 3673–3683
12 Marquardt, D. W. (1963) An algorithm for least squares estimation of nonlinear parameters. J. Soc. Ind. Appl. Math. **11**, 431–441
13 Ros, R., Lemaillet, G., Fonrouge, A. G., Daram, P., Enjuto, M., Salmon, J. M., Thibaud, J. B. and Sentenac, H. (1999) Molecular determinants of the *Arabidopsis* AKT1 K^+ channel ionic selectivity investigated by expression in yeast of randomly mutated channels. Physiol. Plant **105**, 459–468
14 Minet, M., Dufour, M. E. and Lacroute, F. (1992) Complementation of *Saccharomyces cerevisiae* auxotrophic mutants by *Arabidopsis thaliana* cDNAs. Plant J. **2**, 417–422
15 Dreyer, I., Poree, F., Schneider, A., Mittelstadt, J., Bertl, A., Sentenac, H., Thibaud, J. B. and Mueller-Roeber, B. (2004) Assembly of plant *Shaker*-like K_{out} channels requires two distinct sites of the channel alpha-subunit. Biophys. J. **87**, 858–872
16 Gajdanowicz, P., Garcia-Mata, C., Gonzalez, W., Morales-Navarro, S. E., Sharma, T., González-Nilo, F. D., Gutowicz, J., Mueller-Roeber, B., Blatt, M. R. and Dreyer, I. (2009) Distinct roles of the last transmembrane domain in controlling *Arabidopsis* K^+ channel activity. New Phytol. **182**, 380–391
17 Riedelsberger, J., Sharma, T., Gonzalez, W., Gajdanowicz, P., Morales-Navarro, S. E., Garcia-Mata, C., Mueller-Roeber, B., González-Nilo, F. D., Blatt, M. R. and Dreyer, I. (2010) Distributed structures underlie gating differences between the K_{in} channel KAT1 and the K_{out} channel SKOR. Mol. Plant **3**, 236–245
18 Phillips, J. C., Braun, R., Wang, W., Gumbart, J., Tajkhorshid, E., Villa, E., Chipot, C., Skeel, R. D., Kale, L. and Schulten, K. (2005) Scalable molecular dynamics with NAMD. J. Comput. Chem. **26**, 1781–1802
19 MacKerell, Jr, A. D., Bashford, D., Bellott, M., Dunbrack, Jr, R. L., Evanseck, J., Field, M. J., Fischer, S., Gao, J., Guo, H., Ha, S. et al. (1998) All-atom empirical potential for molecular modeling and dynamics studies of proteins. J. Phys. Chem. B **102**, 3586–3616
20 Humphrey, W., Dalke, A. and Schulten, K. (1996) VMD: visual molecular dynamics. J. Mol. Graphics **14**, 33–38
21 Casasnovas, R., Frau, J., Ortega-Castro, J., Salva, A., Donoso, J. and Munoz, F. (2009) Absolute and relative pK_a calculations of mono and diprotic pyridines by quantum methods. J. Mol. Struct.: THEOCHEM **912**, 5–12
22 Liptak, M. D. and Shields, G. C. (2001) Accurate pK_a calculations for carboxylic acids using complete basis set and Gaussian-n models combined with CPCM continuum solvation methods. J. Am. Chem. Soc. **123**, 7314–7319
23 Lim, C., Bashford, D. and Karplus, M. (1991) Absolute pK_a calculations with continuum dielectric methods. J. Phys. Chem. **95**, 5610–5620
24 Bryantsev, V. S., Diallo, M. S. and Goddard, W. A. (2007) pK_a calculations of aliphatic amines, diamines, and aminoamides via density functional theory with a Poisson–Boltzmann continuum solvent model. J. Phys. Chem. A **111**, 4422–4430
25 Reference deleted
26 Becke, A. D. (1993) A new mixing of Hartree–Fock and local density-functional theories. J. Chem. Phys. **98**, 1372–1377
27 Tannor, D. J., Marten, B., Murphy, R., Friesner, R. A., Sitkoff, D., Nicholls, A., Honig, B, Ringnalda, M. and Goddard, III, W. A. (1994) Accurate first principles calculation of molecular charge distributions and solvation energies from *ab initio* quantum mechanics and continuum dielectric theory. J. Am. Chem. Soc. **116**, 11875–11882
28 Marten, B., Kim, K., Cortis, C., Friesner, R. A., Murphy, R. B., Ringnalda, M. N., Sitkoff, D. and Honig, B. (1996) New model for calculation of solvation free energies: correction of self-consistent reaction field continuum dielectric theory for short-range hydrogen-bonding effects. J. Phys. Chem. **100**, 11775–11788
29 Pilot, G., Lacombe, B., Gaymard, F., Chérel, I., Boucherez, J., Thibaud, J. B. and Sentenac, H. (2001) Guard cell inward K^+ channel activity in *Arabidopsis* involves expression of the Twin channel subunits KAT1 and KAT2. J. Biol. Chem. **276**, 3215–3221
30 Minoux, H. and Chipot, C. (1999) Cation–π interactions in proteins: can simple models provide an accurate description? J. Am. Chem. Soc. **121**, 10366–10372
31 Gallivan, J. P. and Dougherty, D. A. (1999) Cation–π interactions in structural biology. Proc. Natl. Acad. Sci. U.S.A. **96**, 9459–9464

32 Dougherty, D. A. (2007) Cation–π interactions involving aromatic amino acids. J. Nutr. **137**, 1504S–1508S
33 Wintjens, R., Lievin, J., Rooman, M. and Buisine, E. (2000) Contribution of cation–pi interactions to the stability of protein–DNA complexes. J. Mol. Biol. **302**, 395–410
34 Bruice, T. C. and Schmir, G. L. (1958) Imidazole catalysis. II. The reaction of substituted imidazoles with phenyl acetates in aqueous solution. J. Am. Chem. Soc. **80**, 148–156
35 Starkus, J. G., Varga, Z., Schnherr, R. and Heinemann, S. H. (2003) Mechanisms of the inhibition of *Shaker* potassium channels by protons. Pflugers Arch. **447**, 44–54
36 Niemeyer, M. I., González-Nilo, F. D., Zúñiga, L., González, W., Cid, L. P. and Sepúlveda, F. V. (2006) Gating of two-pore domain K^+ channels by extracellular pH. Biochem. Soc. Trans. **34**, 899–902
37 Niemeyer, M. I., González-Nilo, F. D., Zúñiga, L., González, W., Cid, L. P. and Sepúlveda, F. V. (2007) Neutralization of a single arginine residue gates open a two-pore domain, alkali-activated K^+ channel. Proc. Natl. Acad. Sci. U.S.A. **104**, 666–671

Received 18 August 2011/13 October 2011; accepted 10 November 2011
Published as BJ Immediate Publication 10 November 2011, doi:10.1042/BJ20111498

38 Zúñiga, L., Márquez, V., González-Nilo, F. D., Chipot, C., Cid, L. P., Sepúlveda, F. V. and Niemeyer, M. I. (2011) Gating of a pH-sensitive K(2P) potassium channel by an electrostatic effect of basic sensor residues on the selectivity filter. PLoS ONE **6**, e16141
39 Liu, J., Zhang, M., Jiang, M. and Tseng, G. N. (2002) Structural and functional role of the extracellular S5-P linker in the HERG potassium channel. J. Gen. Physiol. **120**, 723–737
40 Pilot, G., Pratelli, R., Gaymard, F., Meyer, Y. and Sentenac, H. (2003) Five-group distribution of the *Shaker*-like K^+ channel family in higher plants. J. Mol. Evol. **56**, 418–434
41 Thompson, A. N., Posson, D. J., Parsa, P. V. and Nimigean, C. N. (2008) Molecular mechanism of pH sensing in KcsA potassium channels. Proc. Natl. Acad. Sci. U.S.A. **105**, 6900–6905
42 Hoth, S., Geiger, D., Becker, D. and Hedrich, R. (2001) The pore of plant K^+ channels is involved in voltage- and pH-sensing: domain-swapping between different K^+ channel α-subunits. Plant Cell **13**, 943–952